THE BUOYANCY OF A GAS BUBBLE IN A TUBE FILLED WITH A VISCOUS LIQUID

P. K. Volkov

UDC 532.529.6

A numerical study has been undertaken in this project of the problem revolving around the steady-state motion of a gas bubble in a viscous incompressible liquid in a vertical tube, where the distance between the walls of the bubble and the tube may be small. For Reynolds numbers Re ≤ 100 we have obtained the characteristics of the flow and the shape of the bubble surface. We have observed that in the case in which Re > 60, given the compressed conditions in the trailing portion of the bubble, a dead zone is formed at the tube wall. Diagrams of the flow regimes have been constructed on the basis of the numerical calculation data.

1. Formulation of the Problem. Let us take a vertical tube of radius R_t, filled with a viscous incompressible liquid at rest. The force of gravity acts from the top down. Thus, if we cause a gas bubble to enter the tube (or if we produce this gas bubble by means of an electric discharge), the bubble will float to the top under the force of Archimedes buoyancy. If the volume, shape, and rate of ascent do not undergo significant change over some segment of bubble motion in this case, we can then assume that the bubble is engaged in steady-state motion. As demonstrated by numerous experiments, the segment of non-steady-state motion in a number of cases is small and in actual installations a quasisteady buoyancy regime is quickly established. We should take note of the fact that the buoyancy rate u under these conditions is defined by the parameter and depends on the volume V, the surface shape, and the flow of the liquid around the bubble.

The mathematical description is conveniently carried out in a coordinate system connected to the "center" of the bubble. Within this system the gas bubble is at rest and the liquid impinges on the bubble and at some distance from the bubble exhibits a velocity equal to u (Fig. 1). Let us introduce the coordinate system (r, θ, φ) with its origin O at the "center of the bubble." In the case of axisymmetric flow the Navier–Stokes equations in the variables of the vortex ω and the stream function ψ [1] have the form

$$D^2\psi = -2r\sin\theta\omega; \tag{1.1}$$

$$D^2\omega = \frac{\nu}{r^2\sin\theta}\left[\psi_\theta\omega_r - \psi_r\omega_\theta - \frac{\omega}{r}\psi_\theta + \omega\operatorname{ctg}\theta\psi_r\right] - \frac{2}{r}\omega_r + \frac{\omega}{r^2\sin^2\theta} - \frac{2\operatorname{ctg}\theta}{r^2}\omega_\theta \tag{1.2}$$

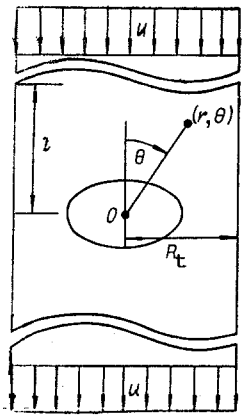

Fig. 1

Novosibirsk. Translated from Zhurnal Prikladnoi Mekhaniki i Tekhnicheskoi Fiziki, Vol. 30, No. 6, pp. 98-105, November-December, 1989. Original article submitted July 12, 1988.

0021-8944/89/3006-0928$12.50

$$\left(D^2 \equiv \frac{\partial^2}{\partial r^2} + \frac{\sin\theta}{r^2}\frac{\partial}{\partial\theta}\left(\frac{1}{\sin\theta}\frac{\partial}{\partial\theta}\right) - \text{Stokes operator}\right).$$

Let us specify the boundary-value conditions: a) at the surface of the bubble Γ ($r = R(\theta)$, $\theta \in [0, \pi]$)

the condition of nonpenetration

$$\psi(r, \theta) = 0; \tag{1.3}$$

equality of tangential stresses to zero

$$\omega + \frac{R^2 + 2R'^2 - RR''}{R^2 + R'^2}\frac{\psi_r}{r^2\sin\theta} = 0; \tag{1.4}$$

equality of the difference between the normal stresses to the capillary forces

$$-p(r, \theta) + 2\rho\nu\left[\frac{\psi_{\theta r} - \psi_\theta/r + R'\psi_{rr}}{r^2\sin\theta} + \frac{R'}{R}\omega\right] = -p_g + \sigma K$$
$$\left(K = \frac{R^2 + 2R'^2 - RR''}{(R^2 + R'^2)^{3/2}} + \frac{|R'\cos\theta - R\sin\theta|}{R\sin\theta(R^2 + R'^2)^{1/2}} - \text{curvature } \Gamma,\right. \tag{1.5}$$

ν, coefficient of kinematic viscosity; ρ, liquid density; σ, coefficient of surface tension; $p = q - \rho g r\cos\theta + p_\infty$ [$p_\infty = p(r = R_t, \theta = \pi/2)$], pressure in the liquid; q, generalized pressure; p_g, gas pressure in the bubble, assumed to be constant);

b) at the tube wall [$r = G(\theta)$, $\theta \in [\theta^*, \pi - \theta^*]$, $\theta^* = \arctan(R_t/\ell)$, ℓ, length of moving-tube segment under consideration]

adhesion condition

$$\frac{1}{r}\frac{\partial\psi}{\partial r} + \frac{\cos\theta}{r^2\sin\theta}\frac{\partial\psi}{\partial\theta} = -u; \tag{1.6}$$

nonpenetration condition

$$\psi(r, \theta) = -(u/2)r^2\sin^2\theta; \tag{1.7}$$

c) at the tube axis ($\theta = 0$, $\theta = \pi$) the conditions of symmetry

$$\psi(r, \theta) = \omega(r, \theta) = 0; \tag{1.8}$$

d) at the tube inlet ($r = F_1(\theta)$, $\theta \in [0, \theta^*]$) and at the outlet ($r = F_2(\theta)$, $\theta \in [\pi - \theta^*, \pi]$), the conditions of an unperturbed flow

$$\psi_i = -(u/2)r^2\sin^2\theta, \ \omega_i = 0 \ \ (i = 1, 2). \tag{1.9}$$

2. Dimensional Analysis. Equations (1.1)-(1.9) contain six independent parameters:

$$\rho, \ \nu, \ \sigma, \ g, \ p_\infty - p_g, \ \ R_t. \tag{2.1}$$

As we can see from (1.5), the solution depends only on the difference between the pressures p_g within the bubble and p_∞ at infinity. The first five parameters specify the medium and characterize its properties, while the sixth parameter established the geometry of the region occupied by this medium. According to dimensional theory, three independent dimensionless criteria exist. Various methods may be used to make these criteria dimensionless. In the course of an experiment, as a rule, the bubble volume V is easily specified (and this applies equally to any linear dimension $a = \sqrt[3]{3V/4\pi}$). Moreover, since in this formulation the liquid at some distance from the bubble moves at a constant velocity $-u$, as the characteristic dimensions and velocities for the procedure of making the criteria dimensionless we can take a and u. We should remember that in (2.1) any two parameters become determinable. In the present study these will be g and $p_g - p_\infty$.

Assuming $r = 2ar'$, $\psi = (2a)^2u\psi'$, $\omega = (u/2a\omega')$, $R = 2aR'$, $q = \rho u^2q'$, in analogy with [1] we obtain the following dimensionless parameters: $Re = u2a/\nu$, the Reynolds number; $We = \rho u^2 2a/\sigma$, the Weber number; $Fr = u^2/ga$, the Froude number; $P_d = (p_g - p_\infty)2a/\sigma$, pressure. As the characteristics of the geometry of the flow region, we can conveniently take a look

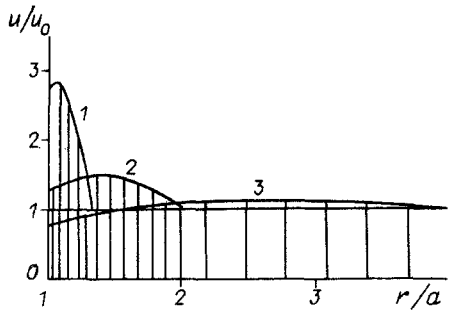

Fig. 2

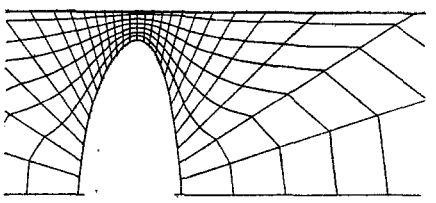

Fig. 3

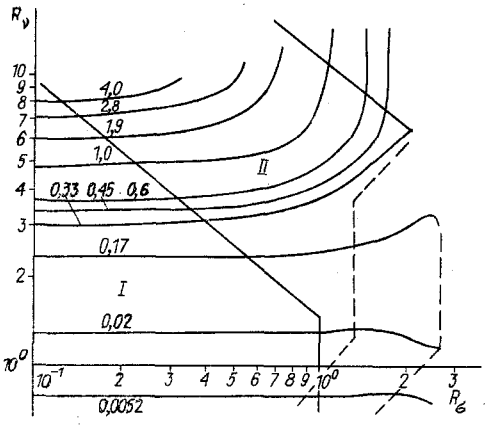

Fig. 4

at the quantity $\lambda = a/R_t$, which is contained in the equation describing the boundaries of the flow region.

3. Transformation of Coordinates and the Method of Solution. Equations (1.1)-(1.9) provide a closed system for the determination of the flow functions and the surface shape of the bubble. Theoretical studies of the validity of this class of problems can be found in [2]. Since the flow region is not known in advance, direct numerical calculation involves considerable difficulties. To overcome these difficulties, we will change to a coordinate system in which the flow region is known. Let us introduce

$$\eta = (r - Q(\theta))/(R(\theta) - Q(\theta)), \quad \theta' = \theta. \tag{3.1}$$

Here $Q(\theta)$ denotes the equation for the boundary containing the inlet to the tube, the outlet from, and the wall of the tube. Transformation (3.1) changes the flow region into a rectangle $[0, 1] \times [0, \pi]$. In these new variables the original equations are more complex in form, but this is offset by the fact that the flow region is known [1, 3].

The algorithm and the method of numerical solutions are analogous to those covered in [1]. The algorithm was tested in the following manner. For $\lambda = 0.2$ the calculations were performed with various values for We, Re, and $\omega = 0$ when $r = Q$. The solutions coincided with those from [1]. As shown by the experiments, even when $\lambda = 0.1$ the influence of the walls on the buoyancy of the bubble is virtually insignificant. It turned out that [4] when $\lambda < 0.2$ for $1 < Re < 40$ the solutions are in agreement with [1].

Solutions have been found in [5] for the problem in which $Re < 0.2$ by the method of expanding the functions over the small parameter and comparison against experiment was carried out. Figure 2 shows a comparison of the derived velocity profiles in the equatorial plane for $\lambda = 0.75$, 0.5, and 0.25 (lines 1-3) with those calculated in [5]. The velocities are virtually coincident.

The parameter $\ell = 10$ has been chosen from the results of the test calculations and undergoes no further change. The characteristic form of the calculation grid in the original coordinate system can be seen in Fig. 3. It is rather small near the bubble, but in the

space between the bubble and the wall, at some distance from the bubble, it becomes larger. On the whole, a grid of this type is useful because it allows us to obtain solutions of problems for values of λ, close to unity, when the distance between the tube walls and the bubble is small. On the other hand, it does have its shortcomings. We should remember that with large values of ℓ it may turn out that no single theoretical point will enter the segment containing the inlet to or the outlet from the tube. This imposes limitations on the interval for the variable θ. In these calculations no less than three points entered the segment containing the inlet or the outlet.

The original problem has three independent dimensionless parameters. In order to obtain complete information regarding the possible flow regimes, we require a considerable number of calculations. In turn, in order to extract from this extensive volume of information and to present in sufficiently usable form the data describing the flows, the derived calculation results must be subjected to appropriate processing. It developed that it was convenient to perform these calculations, provided that Re, We, and λ were chosen as the independent parameters. With a fixed λ we were able to obtain solutions for various Re and We, as in [1]. Changing λ, it became possible to develop a considerable amount of information regarding the flows. The attempt to systematize this information by means of well-established methods (construction of flow-regime diagrams in Re and We coordinates, or Re, $E = \rho g(2a)^2/\sigma$ [6], or $N_V = u^4\sqrt{\rho/g\sigma}$, $N_b = \sqrt{E}$ [7]) does not yield the desired result, since in each of these the coordinates are dependent on the velocity of bubble ascent, which is unknown in advance and, moreover, it is markedly affected by the parameter λ.

Most convenient for this purpose are the coordinates $R_\sigma = a/\sqrt{\sigma/\rho g}$, $R_\nu = a/\sqrt[3]{\nu^2/g}$ [8, 9]. Since R_σ and R_ν depend on the characteristic dimension a of the bubble, having constructed, for example, the Fr isolines in these variables, it is possible very simply to find the rate of ascent for a bubble of a given dimension and to observe the features of the flow for a given liquid, since the Morton number $M = g\nu^4\rho^3/\sigma^3 = (R_\sigma/R_\nu)^6$, and this means that each medium is represented in the coordinates R_σ, R_ν by some straight line whose slope is defined by M.

The calculations were carried out for three values of λ, and for each of these in the case of Re = 0.1-100 a series of calculations were carried out for $We = 10^{-7}$-3.3.

4. Moderate Influence of the Walls ($\lambda = 0.5$). Figure 4 shows the Fr isolines in the coordinates R_σ and R_ν. The lower left-hand angle I, bounded by the solid line, represents the region of spherical bubbles. The level lines are virtually straight lines parallel to the R_σ axis. This means that the rate of ascent depends exclusively on R_ν. We observe a linear relationship between Fr and Re: $Fr = k_1 Re$ ($k_1 = 0.05$). In region II, contained between the two solid lines, the bubble shapes are other than spherical. The Fr isolines are distorted, and we observe two variations in their behavior. In the upper portion of region II the Fr isolines extend to the straight lines parallel to the R_ν axis, i.e., the flow depends on the single parameter R_σ, while in the lower region II the Fr isolines exhibit a tendency to monotonic diminution with an increase in R_σ. This behavior on their part is a reflection of the diverse nature of bubble deformation. Thus, in the upper portion of region II the bubbles undergo flattening, and they are drawn out across the flow, as in the case of an "unlimited volume" [1]. Everywhere above the upper rectilinear boundary of region II we find a closed wake behind the bubble: the bubble and a part of the liquid are streamlined by the liquid flow. The changes in the deformation of the bubble lead to a situation in which the relationship between the bubble region and the region of the wake changes with a relatively small change in the external boundary of this formation. In Fig. 5a (Re = 60, We = 2.57, $M = 6.4\cdot10^{-6}$, $R_\sigma = 1.72$, $R_\nu = 12.6$) we see a characteristic flow pattern with the isolines of the stream function represented at the bottom and the liquid velocity field through the cross section of the tube shown at the top. The left-hand dashed line in Fig. 4 indicates that the frontal portion of the bubble is deformed by an upstream protrusion while the right-hand dashed line indicates that the trailing portion of the bubble is elongated downstream. Thus, the deformation of the bubble in the lower portion of region II comes about as a consequence of elongation of the bubble along the axis of the tube. Figure 5b (Re = 0.1, We = 0.065, M = 954, $R_\sigma = 2.44$, $R_\nu = 0.78$) shows the flow pattern for this case, while Fig. 5c (Re = 20, We = 3.18, M = 0.001, $R_\sigma = 2.16$, $R_\nu = 6.74$) shows the flow pattern which corresponds to a region intermediate between these two sections. The bubble has a shape reminiscent of a lens. Despite the fact that the trailing portion is flat, the flow here undergoes no detachment. The velocity profile through the cross section of the tube exhibits differences throughout only in a small zone near the bubble. The fric-

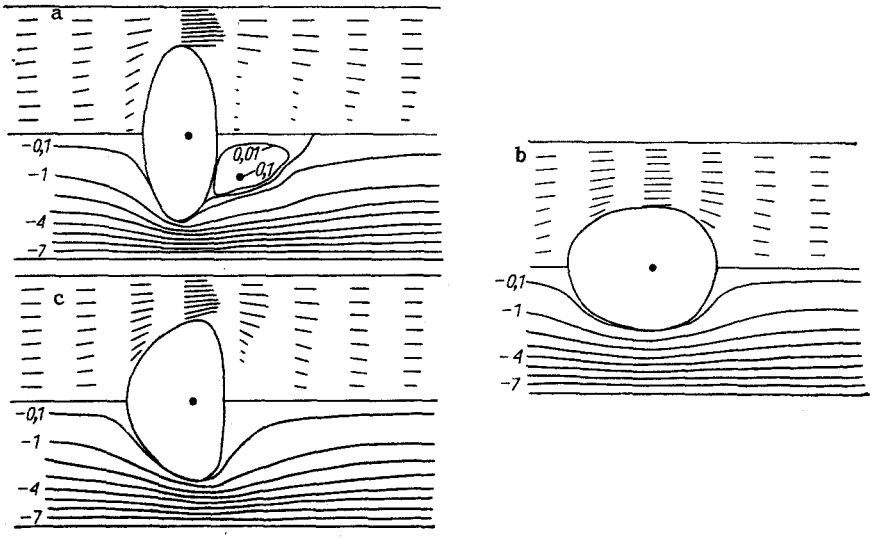

Fig. 5

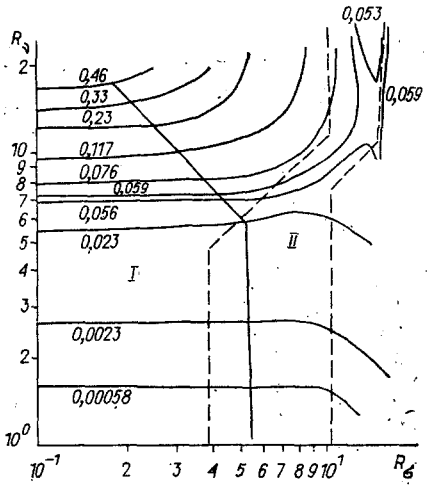

Fig. 6

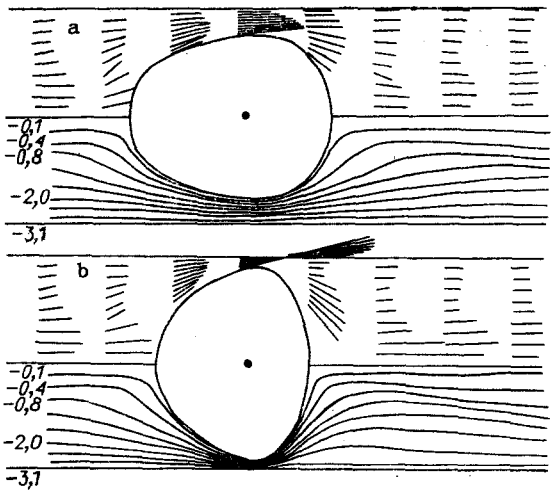

Fig. 7

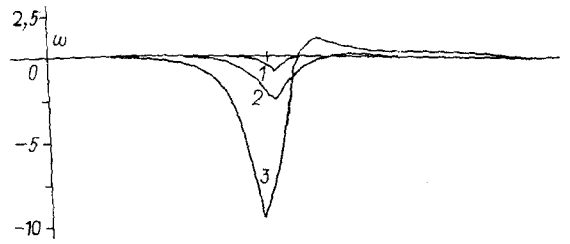

Fig. 8

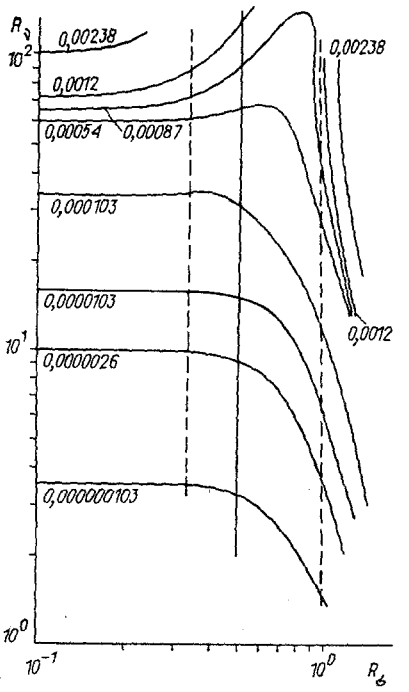

Fig. 9

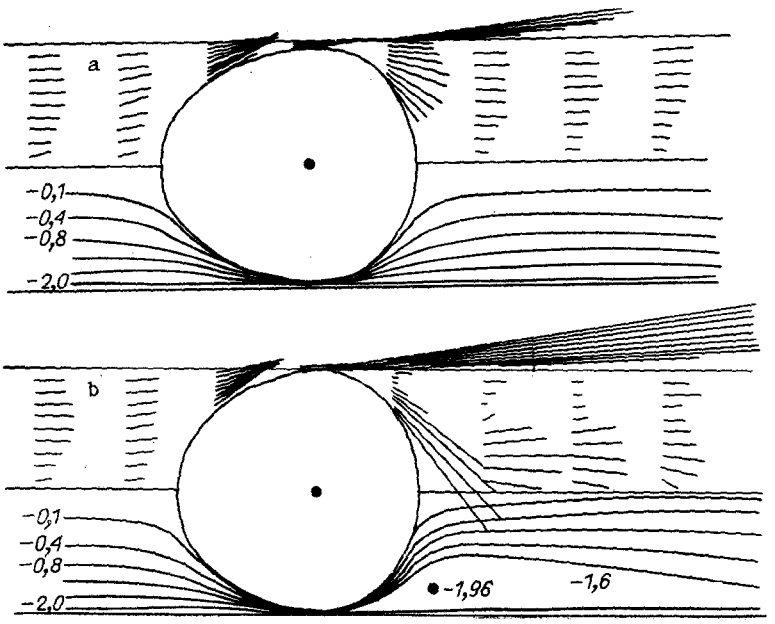

Fig. 10

tion at the tube wall which coincides with the function $2\omega/Re$ is insignificant and it is negative along the line of the bubble, which suggests acceleration of the liquid here, and the friction both in front and behind the bubble is positive.

5. Strong Influence of the Walls ($\lambda = 0.8$). Figure 6 shows the Fr isolines in the coordinates R_σ and R_ν. The flow regime diagram, on the whole, has the same structure as in the case of $\lambda = 0.5$, but shifted upward. The left-hand lower corner I, identified by the bent solid line, represents the region of spherical bubbles. The value of Fr undergoes virtually no change as R_σ increases and depends linearly on $Re:Fr = k_2 Re$ ($k_2 = 0.00575$). In region II the flow is determined by the parameters R_σ and R_ν. The dashed lines indicate the nature of bubble deformation. The extension of the bubble along the axis leads to an increase in the gap between the walls of the tube and the bubble. A characteristic flow pattern can be found in Fig. 7a (Re = 0.4, We = 0.019, M = 0.148, $R_\sigma = 1.63$, $R_\nu = 2.24$). In the upper portion of region II the bubble is wedge-shaped (Fig. 7b, Re = 60, We = 0.19,

$M = 2.3 \cdot 10^{-8}$, $R_\sigma = 1.42$, $R_\nu = 26.7$). The gap between the walls of the tube and the bubble is made smaller, becoming shortened in the axial direction. In each of these cases the flows are distinguished only in a small region near the bubble. The liquid is accelerated at the axis of the tube, and at some distance from the wall we observe a zone of decelerated flow. Figure 8 shows the distribution of the vortex ω at the wall of the tube: 1) Re = 0.4, We = 0.019, M = 0.148; 2) Re = 20, We = 0.36, $M = 8.2 \cdot 10^{-6}$; 3) Re = 60, We = 0.19, $M = 2.3 \cdot 10^{-8}$. As the gap between the walls of the tube and the bubble is reduced, the negative peak in ω increases sharply, i.e., the liquid is accelerated. Immediately behind the narrow portion of the gap ω changes sign to the positive, i.e., the liquid is decelerated at the wall in an expanding flow. In the narrow band of region II (see Fig. 6), where the bubble deformation process is restructured, the Fr isolines correspond to the contour lines of the saddle surface. This means that the relationship between the rate of bubble ascent and its dimensions will be nonmonotonic in nature.

The increase in bubble dimensions leads to an increase in the rate of ascent only when the deformation of the bubble is caused by its extension along the axis of the tube. The friction at the wall characterizes the extent of "tube blockage."

6. The "Plug" Flow Regime ($\lambda = 0.98$). Calculations for values of λ close to unity apparently are of only theoretical interest, since in actual practice in these cases tube "blockage" occurs. The presence of irregularities on the wall and the vaporization process at the free surface, which may be decisive in the given case, lead to a situation in which the thin liquid film between the walls of the tube and the bubble breaks down.

Figure 9 shows the flow regime diagrams in the coordinates R_σ and R_ν. The nature of the Fr isolines is the same as in Figs. 4 and 6. The region of their nonmonotonic change has been raised even higher. To the left of the straight line $R_\sigma = 0.5$ we have the region in which spherical bubbles exist. The dashed lines indicate the nature of bubble deformation. Thus, when $R_\sigma > 1$ the deformation of the surface takes place as a result of surface elongation in the direction of the flow, with an enlargement of the space between the walls of the tube and the bubble. In the spherical bubble region Fr is proportional to Re: $Fr = k_3 Re$ ($k_3 = 0.0000257$). The rate of bubble ascent is very small: $u = \sqrt{g a Fr}$. For many liquids $\delta_\sigma = \sqrt{\sigma/\rho g} = 0.0015 - 0.003$ m, when $R_\sigma = 0.5$, $a = 0.5\delta_\sigma$. Substituting all of this information into the formula for the velocity yields $u = \sqrt{9.8 \cdot 0.5 \delta_\sigma Fr}$. When $R_\nu = 10$, $Fr = 0.03 \cdot 10^{-4}$ and u ~ 0.15 mm/sec.

Figure 10a (Re = 0.004, $We = 2.1 \cdot 10^{-6}$, M = 0.0813, $R_\sigma = 1.12$, $R_\nu = 1.71$) shows the pattern of the flow around a bubble when Re = 0.004. Despite the fact that Re and We are small here, the bubble surface is deformed. An increase in Re leads to a reduction in the gap between the walls of the tube and the bubble. The most significant differences from Fig. 10a are observed behind the bubble, at a distance equal approximately to the diameter of the tube. A zone of decelerated flow arises here in the vicinity of the wall, and near the bubble surface and the tube axis a liquid jet is formed, which, by the way, undergoes rapid deceleration. Figure 10b shows the flow for the case in which Re = 60, We = 0.0024, $M \sim 10^{-12}$, $R_\sigma = 1.08$, $R_\nu = 94.65$. At the wall behind the bubble we note the formation of flow with closed streamlines, i.e., a toroidal vortex. A liquid jet exists between the bubble and this vortex, moving at a velocity considerably greater than the bubble rate of ascent, and it is directed toward the axis of the tube. With Re = 100 the flow pattern becomes more complex. At the tube wall behind the bubble we now have two vortices rotating in different directions. Figure 11 shows the graphs for the distribution of ω at the wall of the tube : 1) Re = 0.004, $We = 2.1 \cdot 10^{-6}$, $R_\sigma = 1.12$, $R_\nu = 1.71$; 2) Re = 40, We = 0.0053, $R_\sigma = 1.14$, $R_\nu = 58.2$; 3) Re = 100, We = 0.00032, $R_\sigma = 0.26$, $R_\nu = 102.4$; 4) Re = 60, We =

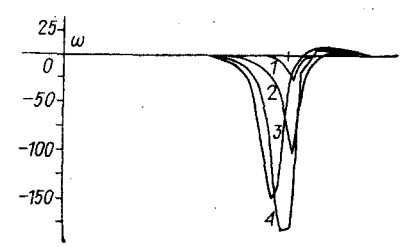

Fig. 11

0.0024, $R_\sigma = 1.08$, $R_\nu = 94.65$. In the region where Re < 60 (see Fig. 9) where the Fr isolines are monotonic or exhibit a slight local maximum, the peak in the modulus of ω diminishes as R_σ increases (the gap is enlarged). With Re > 60 in the zone bounded by the dashed lines, the flow and the deformation of the surface proceed in a manner such that the peak of the modulus of ω at the wall becomes even larger.

7. Discussion of Results. The flow regime diagrams shown in Figs. 4, 6, 9 and the flow diagrams (Figs. 5, 7, 10) provide some idea as to the process of bubble buoyancy and the influence of the walls on the flow. The presence in this problem of the parameter λ prevents us from constructing the relationship between the rate of bubble ascent and the dimensions of the bubble in a tube with the given radius as easily as in the case of an unlimited liquid volume. To achieve this goal it is essential that we have a significantly larger number of diagrams with various values of λ. Here, on the other hand, we can obtain only three points on this relationship. In tubes of small radius the increase in bubble dimension may lead to the "blockage" of the tube. Only when $R_\sigma > 1$ will the increase in the volume of the bubble lead to an increase in the rate of bubble ascent.

Attempts to obtain results for R_σ larger than indicated on the diagrams led to a situation in which the bubble frequently began to grow, becoming elongated in the direction of the axis. The iteration process converged, but for another value of λ. Increased accuracy of calculation or a larger number of nodes in the calculation grid, on the whole, did not eliminate this problem. This may possibly be associated with the fact that a "plug" flow regime set in, or one close to it, practically defining both the flow in which the rate of bubble ascent no longer depends on bubble volume. Taking into consideration the presence of nonsteadiness at the free surface under specific conditions, we can ascribe another explanation to this phenomenon.

Comparison of the diagrams in Figs. 4, 6, and 9 with ones analogous from [9] shows their good agreement in the region $R_\sigma > 1$. With $R_\sigma < 1$ we have considerable divergences associated with the presence of surface-active substances (SAS) in the experiment. As was demonstrated earlier [8], if we were able to rid ourselves of the SAS, the comparison of the experimental and theoretical data would also be satisfactory for the case in which $R_\sigma < 1$.

The calculation results presented here are in qualitative agreement with the experimental data from [10], where the longitudinal component of the velocity profile through the cross section of the tube and the friction at the wall were measured as part of the problem dealing with plug-flow motion of a string of bubbles.

LITERATURE CITED

1. C. I. Christov and P. K. Volkov, "Numerical investigation of the steady viscous flow past a stationary deformable bubble," J. Fluid Mech., 158, 341 (1985).
2. V. V. Pukhnachev, "Problems related to free boundaries for Navier–Stokes equations," Doctoral Dissertation, Physicomathematical Sciences, IT SO Akad. Nauk SSSR, Novosibirsk (1974).
3. P. K. Volkov and B. G. Kuznetsov, "Numerical solution of the problem of steady-state streamlining of a gas cavity in a tube with a viscous liquid," ChMMSS, 13, No. 5 (1982).
4. P. K. Volkov and B. G. Kuznetsov, "Boundary conditions for the problem of streamlining a bubble with a viscous liquid," in: Numerical Simulation in Fluid Dynamics [in Russian], ITPM SO Akad. Nauk SSSR, Novosibirsk (1983).
5. M. Coutanceau and P. Thizon, "Wall effect on the bubble behavior in highly viscous liquids," J. Fluid Mech., 107, 339 (1981).
6. D. Bhaga and M. E. Weber, "Bubbles in viscous liquids: shapes, wakes, and velocities," J. Fluid Mech., 105, 61 (1981).
7. J. H. C. Coppus and K. Rietema, "Description of bubble shape in terms of dimensionless number," Chem. Engng. Sci., 35, No. 6 (1980).
8. P. K. Volkov and E. A. Chinnov, "Buoyancy of spherical and ellipsoidal bubbles in an unbounded liquid volume," in: The Hydrodynamics and Acoustics of One- and Two-Phase Flows [in Russian], IT SO Akad. Nauk SSSR, Novosibirsk (1983).
9. E. A. Chinnov, "Studying the effect of walls in a cylindrical vertical channel on the rate of ascent for individual gas bubbles," in: The Thermophysics and Hydrodynamics of Boiling and Condensation Processes [in Russian], IT SO Akad. Nauk SSSR, Novosibirsk (1985).

10. V. E. Nakoryakov, O. N. Kashinsky, and B. K. Kozmenko, "Experimental study of gas–liquid slug flow in a small-diameter vertical pipe," Int. J. Multiphase Flow, 12, No. 3 (1986).

THE KINETIC MODEL OF A CARRIER PHASE IN A HETEROGENEOUS MEDIUM

Yu. E. Gorbachev

UDC 533.7

To describe a rarefied gas suspension we normally make use of a system of Boltzmann equations (BE), written for each of the components (see the review in [1]). Regimes which allow for such a description are examined in [2] and these are characterized by a system of inequalities (i, j = 1, 2): $r_i \ll d_i$, $\max r_i \lesssim \ell_j$ $(j \neq i)$, where r_i denotes the radii of the mixture components, $d_i = n_i^{-1/3}$, n_i, ℓ_i is the numerical density and the mean free path of the i-th component $[\ell_i \sim (r_i^2 n_i)^{-1}]$. In [3-6] we find a method for the solution of this system through various Enskog–Chapman (ECh) modifications.

Among the advantages in studying systems described by BE is the utilization of kinetic models. With this approach consideration of the complex physicochemical processes occurring at the surface of a particle is reduced to the calculation of the appropriate coefficients of the model (expressed in terms of the exchange coefficients), as well as the transition to the macroscopic description (including the derivation of expressions for the transfer coefficients) are realized considerably more simply than in the solution of the complete BE by the ECh method. The different versions of these kinetic models for mixtures were studied in [2, 7-9]. In the present study we examine the question of the construction of a kinetic model for the light component and its analysis within the framework of the ECh method, given an arbitrary function for the distribution of the heavy component.

The following BE system serves as the basis of our study:

$$df_1/dt_1 = J_{11}(f_1, f_1) + J_{12}(f_1, f_2),\ df_2/dt_1 = J_{22}(f_2, f_2) + J_{21}(f_2, f_1),$$

where $d/dt_i = \partial/\partial t + \mathbf{v}_i \cdot \partial/\partial \mathbf{r}$.

Let us examine a heterogeneous mixture characterized by substantial differences in mass and characteristic radii of the components $\varepsilon^2 = m_1/m_2 \ll 1$, $r_1 \ll r_2$. In this case, the reference mass $\mu_{12} \sim m_1$, and in evaluating the scattering cross section it is possible to assume that $\sigma_{11} \sim r_1^2$, $\sigma_{12} \sim r_2^2$, $\sigma_{22} \sim 4\sigma_{12}$.

For the collision terms J_{ij} we will use Boltzmann-type collision integrals written in symmetrized form:

$$J_{ij} = \frac{(m_1 m_2)^3}{\mu_{ij}} \int d\mathbf{v}_j\, d\mathbf{v}_i'\, d\mathbf{v}_j' \delta_{\mathbf{p}} \delta_E \sigma_{ij}^d \left(f_i' f_j' - f_i f_j\right), \tag{1}$$

where $\delta_{\mathbf{p}}$ and δ_E are the delta-functions of the conservation of momentum and of the kinetic energy of the colliding pair; the primes denote that a given quantity belongs to the characteristics of state after collision; σ^d is the differential scattering cross section whose analytical approximations for elastic collisions have been studied in detail in [10]. In particular, in order to calculate the cross section of the collision between the light component and a heavy component, as well as within the heavy component, it was proposed in [11] to describe the corresponding interactions by means of the Kihara potential.

Construction of the kinetic model [i.e., a finite-multiple approximation of integral (1)] involves two stages: the finding of the quasisteady distributions of f_i^0; the expan-

Leningrad. Translated from Zhurnal Prikladnoi Mekhaniki i Tekhnicheskoi Fiziki, Vol. 30, No. 6, pp. 106-114, November-December, 1989. Original article submitted January 6, 1987; revision submitted June 20, 1988.

0021-8944/89/3006-0936$12.50